CHEMISTRY OF MATERIALS

Article

pubs.acs.org/cm

Thermal Behavior of Methylammonium Lead-Trihalide Perovskite Photovoltaic Light Harvesters

Amalie Dualeh,[†] Peng Gao,[†] Sang Il Seok,[‡,§] Mohammad Khaja Nazeeruddin,[†] and Michael Grätzel*[,†]

[†]Laboratory of Photonics and Interfaces, Institute of Chemical Sciences and Engineering, École Polytechnique Fédérale de Lausanne (EPFL), Station 6, 1015 Lausanne, Switzerland

[‡]Division of Advanced Materials, Korea Research Institute of Chemical Technology, 141 Gajeong-Ro, Yuseong-Gu, Deajeon 305-600, Republic of Korea

[§]Department of Energy Science, Sungkyunkwan University, Suwon 440-746, Korea

Supporting Information

ABSTRACT: Recently organic–inorganic hybrid perovskites have attracted attention as light harvesting materials in mesoscopic cells. While a considerable number of deposition and formation methods have been reported for the perovskite crystalline material, most involve an annealing step. As such, the thermal behavior of this material and its individual components is of crucial interest. Here, we examine the thermal properties of the $CH_3NH_3PbX_3$ (X = I or Cl) perovskite using thermogravimetric analysis. The role of the precursors is exposed, and the effect of the formation of excess organic species is investigated. The sublimation behavior of the organic component is intensively scrutinized. Furthermore, differential scanning calorimetry is employed to probe the crystal phase structure, revealing subtle differences depending on the deposition method.

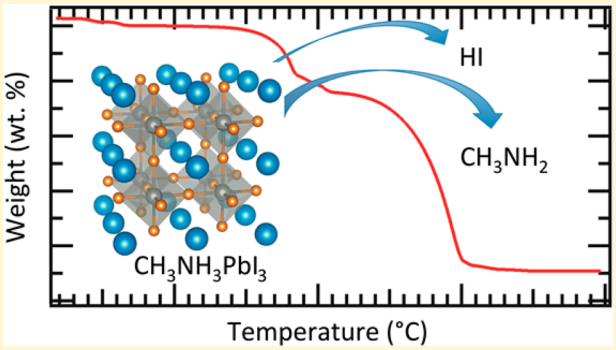

INTRODUCTION

Hybrid organic–inorganic lead-based perovskites represent a class of light absorbing materials whose application in photovoltaics has led to record breaking solar conversion efficiencies of over 17%.[1] These high efficiencies have mainly been achieved using methylammonium lead-halide based perovskites, where the halide is typically iodide[2] or a mixture of iodide and chloride.[3,4] A multitude of different materials,[5−8] device architectures,[3,9,10] and deposition methods[4,11−13] have been reported, demonstrating the versatility of these perovskite materials.

The solution processability of the $CH_3NH_3PbI_3$ perovskite is one of its major advantages. In the simplest method of deposition, a mixture of the precursor materials in a suitable solvent is spin-coated onto the substrate and then subsequently heated at 100 °C. In this deposition method, the molar ratio of the precursors is critical, and its influence on the power conversion efficiency has been reported.[14] The annealing step following deposition of the mixture is required to convert the as-deposited precursor solution to the crystalline perovskite, driving the evaporation of the excess solvent and the crystallization of the perovskite. In previous work, we investigated the role of annealing temperature on the formation of perovskite film from the as-deposited precursor solution.[15] Significant differences in film morphology, composition, and device performance were observed as a function of the annealing temperature. These parameters have proven to be critical to the photovoltaic performance of such perovskite solar cells.[16,17]

In this study, the thermal properties of the perovskite material are examined. The individual components are analyzed in order to correctly identify their contributions to the thermodynamic behavior of the perovskite material formed. Additionally, the formation of the perovskite with the general form $CH_3NH_3PbX_3$ (X = I or Cl) from mixed precursor solutions of PbX_2 and CH_3NH_3X is considered in order to gain insight into the effect of the formation of the excess organic component. This study helps to clarify the role of the precursors' composition used in the perovskite solution mixture.

Thermogravimetric analysis (TGA) is used here to determine the mass loss behavior of the individual organic and inorganic components that make up the building blocks of $CH_3NH_3PbI_3$ as a function of temperature. The sublimation behavior of the isolated organic component is examined in depth and used to interpret the TGA data of various perovskite precursor solutions and of the $CH_3NH_3PbI_3$ powder.

The TGA curves are presented in Figure 1 (parameters in Table S1, Supporting Information). The organic components, CH_3NH_3I and CH_3NH_3Cl, undergo 100% weight loss in one

Received: July 7, 2014
Revised: August 13, 2014
Published: August 15, 2014

   dx.doi.org/10.1021/cm502468k | Chem. Mater. 2014, 26, 6160−6164

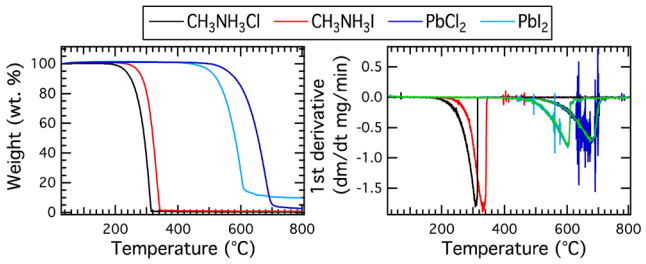

Figure 1. TGA heating curves of individual precursor powders expressed as weight % as a function of applied temperature and the corresponding first derivatives.

step, the onset of which occurs at 234 and 185 °C, respectively, suggesting the sublimation of these materials. This is validated by the sharpness of the transition step in the differential TGA curves. In contrast, the inorganic components, PbI_2 and $PbCl_2$, undergo 90 and 95% weight loss at 646 and 714 °C, respectively. The broad weight loss profile seen in the TGA first derivative imply that these inorganic materials undergo thermal decomposition. This is further highlighted by the tail in the weight % after the material has undergone the majority of its weight loss. The remaining residues may be some decomposition products and/or impurities present in the material. For example, the PbI_2 is purchased at 99% purity and thus contains 1% impurities that may or may not undergo decomposition or evaporation up to 800 °C in N_2.

The direct phase transition from solid to gas (sublimation) ideally involves no compound decomposition. Such thermodynamic processes follow zero-order kinetics resulting in a constant rate of mass loss dm/dt by sublimation at a constant temperature. Hence, dm/dt is linear under isothermal conditions. From the initial TGA heat curves for CH_3NH_3I and CH_3NH_3Cl, the temperature range for sublimation is found to lie between 200 and 350 °C. The temperature of sublimation T_{sub} has been defined as the point at which 20% of mass loss has occurred.[18]

The enthalpy of sublimation ΔH_{sub} can be related to the vapor pressure p and temperature T of the solid using the Clausius−Clapeyron relationship.

$$\ln p = -\frac{\Delta H_{sub}}{R}\left(\frac{1}{T} - \frac{1}{T_{sub}}\right) \quad (1)$$

where R is the gas constant. The assumption is made that ΔH_{sub} is independent of temperature in the range considered here.

The vapor pressure of a material can in turn be related to the mass loss due to sublimation using an expression presented by Langmuir (Supporting Information).[18,19] The instantaneous rate of mass loss m_{sub} at a temperature T can be derived from the TGA first derivative. Using the following equation, the enthalpy ΔH_{sub} and temperature T_{sub} of sublimation can be determined.[20]

$$\ln(m_{sub}T^{1/2}) = -\frac{\Delta H_{sub}}{R}\left(\frac{1}{T} - \frac{1}{T_{sub}}\right) - \frac{1}{2}\ln\left(\frac{2\pi R}{A^2 M_w}\right) \quad (2)$$

where A is the exposed sublimation surface area, and M_w is molecular mass.

Here, it is important to consider the influence of the heating rate used for data acquisition. TGA measurements of CH_3NH_3Cl were performed by heating at different heating rates (10, 5, and 2.5 °C min^{-1}, Figure S1, Supporting Information) and revealed differences in the results obtained. ΔH_{sub} and T_{sub} were calculated for each heating rate using eq 2 (Table S2, Supporting Information). As the heating rate is decreased, the calculated value of ΔH_{sub} decreases from 84.4 ± 0.3 to 79.6 ± 0.4 $kJmol^{-1}$, indicating that fast heating rates lead to an overestimation of this parameter. T_{sub} was determined at approximately 171 °C and found to be relatively insensible to the heating rate. Hence, a more accurate determination of ΔH_{sub} is to consider the isothermal mass loss of the materials.[18]

In order to determine the isothermal mass loss of the organic materials, TGA was run using temperature profiles with multiple isothermal regions of 10 min (Figure S2, Supporting Information). Figure 2a shows the mass loss as a function of time for the different isothermal regions, the linear mass loss at each temperature indicating no additional decomposition. For each isotherm, the slope of the mass loss is determined and can be associated with the rate of mass loss by sublimation m_{sub}.[18] The extracted parameters are presented in Table 1.

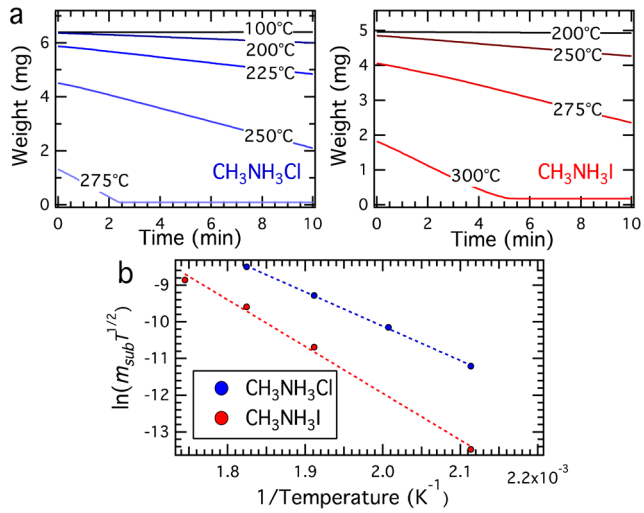

Figure 2. (a) Isothermal mass loss of CH_3NH_3Cl (blue) and CH_3NH_3I (red) determined from TGA. (b) Calculated $\ln(m_{sub}T^{1/2})$ vs $1/T$ for CH_3NH_3Cl (blue) and CH_3NH_3I (red) used to determine ΔH_{sub} and T_{sub}.

Table 1. ΔH_{sub} and T_{sub} of CH_3NH_3Cl and CH_3NH_3I Determined from a Linear Least-Squares Fitting of the TGA Data

precursor	ΔH_{sub} ($kJmol^{-1}$)	T_{sub} (°C)
CH_3NH_3Cl	78 ± 2	195 ± 9
CH_3NH_3I	105 ± 5	247 ± 26

The lower ΔH_{sub} for CH_3NH_3Cl illustrates that it requires less energy to undergo the direct phase transition from solid to gas. This is further reflected in its lower T_{sub}. As such, CH_3NH_3Cl undergoes sublimation more readily than CH_3NH_3I. Furthermore, the value determined for ΔH_{sub} by this isothermal method is in good agreement with that determined from the constant heating technique when the slowest heating rate is used (79.6 ± 0.4 $kJmol^{-1}$). This suggests that this first method can be used to determine this parameter, but to prevent overestimation, a very slow heating rate must be

dx.doi.org/10.1021/cm502468k | Chem. Mater. 2014, 26, 6160−6164

employed. Unlike ΔH_{sub}, which is prone to be overestimated by the constant heating technique, T_{sub} is more accurately determined by this method from the more precisely resolved *y*-intercept.

The deposition of the perovskite is from a solution containing the precursor materials. The precursors investigated are expected to form a pervoskite material of the general formula $CH_3NH_3PbX_3$ (X = Cl or I) according to the following equations.

$$PbX_2 + CH_3NH_3X \rightarrow CH_3NH_3PbX_3 \quad (3)$$

$$PbY_2 + 3CH_3NH_3X \rightarrow CH_3NH_3PbX_3 + 2CH_3NH_3Y \quad (4)$$

Here, we consider the two cases: the formation of the perovskite from (1) a 1:1 molar ratio of precursors based on the same halide (eq 3) or (2) a 1:3 molar ratio mixture where the inorganic and organic components contain different halides (eq 4) and lead to the formation of excess organic material. This is based on the assumption that unlike the iodide−bromide mixed-halide perovskite system,[8] for iodide−chloride mixtures the mixed-halide perovskite of the form $CH_3NH_3PbI_2Cl$ or $CH_3NH_3PbICl_2$ does not exist.[21] Consequently, it is assumed that the perovskite formed depends on the halide of the organic component (Table S3, Supporting Information). An alternate deposition route involves the deposition of PbI_2, which is then converted into the $CH_3NH_3PbI_3$ perovskite by immersion in a solution of excess CH_3NH_3I. This sequential deposition technique is expected to lead to the formation of the same perovskite material as in the single step deposition from a 1 to 1 molar ratio mixture of PbI_2 and CH_3NH_3I. The large differences in the reported solar cell power conversion efficiencies can be attributed to the different perovskite film morphologies, TiO_2 coverage, and the formation of a perovskite capping layer on top of the mesoporous scaffold. The nature and effect of the perovskite film morphology on the thermal properties are outside the scope of this investigation and hence are not further considered.

The TGA of perovskites formed from solution clearly portrays the liberation of the excess organic material for the mixed halide systems (Supporting Information). Furthermore, only the pure chloride system leads to the formation of pure $CH_3NH_3PbCl_3$, evident in the shift of the inorganic decomposition to higher temperatures and confirmed by XRD. For all other mixtures, the main inorganic component is PbI_2.

XRD measurements were conducted to confirm the nature of the perovskite formed from the different perovskite precursor solution mixtures and are presented in Figure 3.

Samples formed from solutions 2 and 3, corresponding to the 1:1 PbI_2 and CH_3NH_3I and 1:3 $PbCl_2$ and CH_3NH_3I mixtures, are observed to show the peaks associated with the expected triiodide perovskite $CH_3NH_3PbI_3$. Solution 4, the pure chloride system (1:1 molar ratio of $PbCl_2$ and CH_3NH_3Cl), clearly displays the XRD diffraction peaks in good agreement to those reported for the trichloride perovskite $CH_3NH_3PbCl_3$.[22] Interestingly, in the case of solution 1, the 1:3 mixture of PbI_2 and CH_3NH_3Cl, only a small peak at 15.7° is visible. This peak is attributed to the (110) reflection for $CH_3NH_3PbCl_3$. Hence, from the XRD diffractogram it is apparent that this mixture does lead to the formation of the $CH_3NH_3PbCl_3$ perovskite, while the TGA measurement suggests the formation of a PbI_2 component (which is, however, not detected by XRD). Hence, it is possible that some mixture of perovskite and precursors is formed, which is predominantly based on the trichloride form (as evident from the XRD data), but which undergoes thermal decomposition to PbI_2 at high temperatures.

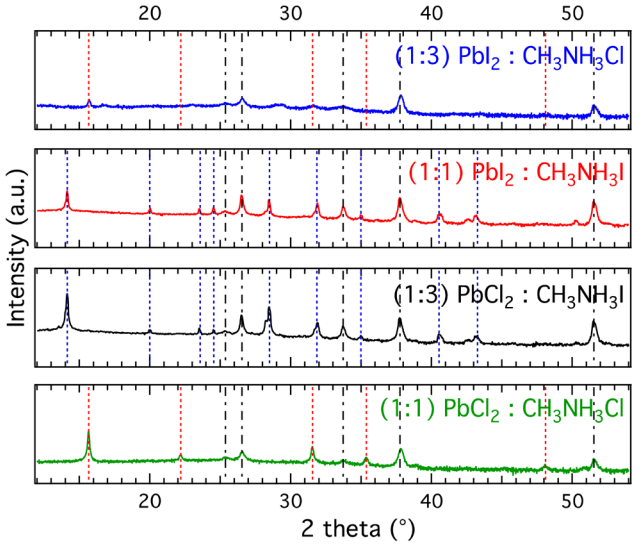

Figure 3. XRD measurements of perovskite films deposited from mixed precursor solutions: solution 1, 1:3 molar ratio of PbI_2 and CH_3NH_3Cl in DMSO (blue); solution 2, 1:1 molar ratio of PbI_2 and CH_3NH_3I in DMF (red); solution 3, 1:3 molar ratio of $PbCl_2$ and CH_3NH_3I in DMF (black; and solution 4, 1:1 molar ratio of $PbCl_2$ and CH_3NH_3Cl in DMSO (green). The vertical lines indicate the peaks associated with triiodide perovskite $CH_3NH_3PbI_3$ (blue), trichloride perovskite $CH_3NH_3PbCl_3$ (red), and the FTO/mTiO_2 substrate (dotted black line).

Figure 4 shows the TGA results for the triiodide perovskite powder formed from solutions of a 1 to 1 molar ratio of the PbI_2 and CH_3NH_3I and a 1 to 3 molar ratio of $PbCl_2$ and CH_3NH_3I in DMF.

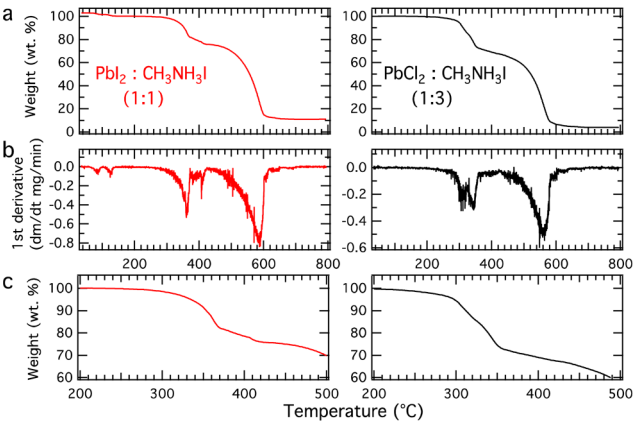

Figure 4. (a) TGA heating curves and (b) corresponding 1st derivatives for the perovskite powders; 1:1 molar ratio of PbI_2 and CH_3NH_3I in DMF (red) and 1:3 molar ratio of $PbCl_2$ and CH_3NH_3I in DMF (black). (c) Magnification of the region for organic mass loss.

The formation of this perovskite was confirmed by XRD (Figure 3). Two small mass losses take place for the solution based on the PbI_2 precursor at 85 and 125 °C, clearly visible as two small minima in the first derivative. These are most likely due to the removal of absorbed H_2O from the perovskite material as has been previously reported.[23] The mass loss step

dx.doi.org/10.1021/cm502468k | *Chem. Mater.* 2014, 26, 6160−6164

between 550 and 600 °C for both samples is in good agreement with the thermal decomposition of the inorganic PbI_2 proportion of the perovskite formed. As was the case for the perovskite solutions, the differences between the samples are mostly in the liberation of the organic material. For the sample prepared from PbI_2, the material undergoes 20% mass loss followed by approximately 5−6% mass loss. This is in excellent agreement with the calculated consecutive loss of the HI species followed by the CH_3NH_2 component. The mass loss step corresponding to the amine is not as clearly defined, resulting in a broader feature in the first derivative. This suggests that this species is not as readily lost as the HI and is more tightly bound to the perovskite matrix, likely by hydrogen bonding. This sequential loss of HI followed by CH_3NH_2 is not observed in the TGA of the pure precursors (cf. Figure 1) confirming that this decomposition pathway occurs only when the organic species is incorporated into the perovskite structure. The pure organic material (CH_3NH_3X) is lost via sublimation in a single mass loss step.

For the perovskite using the $PbCl_2$ precursor, the loss of the organic material occurs in three stages between 250 and 400 °C corresponding to mass losses of 16, 12, and 5%. This is in good agreement with the loss of the excess 2 mol equiv of CH_3NH_3Cl by sublimation, followed by the consecutive loss of HI and CH_3NH_2 from the organic perovskite component. This suggests that the majority of the excess CH_3NH_3Cl formed remains mixed within the perovskite matrix even after heating the sample at 100 °C for 45 min. This was confirmed by isothermal heating of the material at 125 °C for 60 min, which exhibited only approximately 2% mass loss. Similar to the PbI_2 case, the final mass loss of 5% attributed to the loss of the amine constituent is apparent as a slope in the TGA curve between 350 and 400 °C rather than an abrupt mass loss step, confirming the theory that this species is more firmly fixed in the perovskite matrix than the HI component.

Differential scanning calorimetry (DSC) was used to gain further insight into the thermal behavior of the triiodide perovskite (Figure 5). The heating (solid line) and cooling (dashed line) thermograms were recorded consecutively by heating the sample from 30 to 200 °C and cooling down again two times.

In the case of the PbI_2 based perovskite, the thermograms show peaks at 57.3 and 55.2 °C for the heating and cooling scans, respectively, reproduced in the second cycle. These are in very good agreement with the reported tetragonal to cubic phase transition of $CH_3NH_3PbI_3$.[23] The asymmetry of the DSC peaks has been suggested to indicate the presence of a transient intermediate phase but remains relatively unclear.[23]

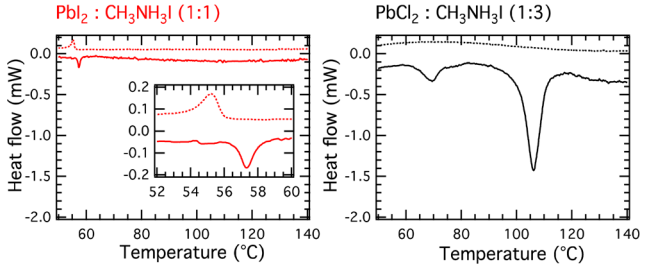

Figure 5. (Left panel) DSC heating (solid trace) and cooling (dashed trace) curves for the perovskite powders heated at 10 °C min^{-1}; 1:1 molar ratio of PbI_2 and CH_3NH_3I in DMF (red). (Right panel) 1:3 molar ratio of $PbCl_2$ and CH_3NH_3I in DMF (black). The DSC scans have been corrected to account for the baseline drift.

For the $PbCl_2$ precursor based perovskite powder, these features between 54 and 58 °C are not detected within the limit of the experiment. This insinuates that subtle differences exist between the perovskite materials formed depending on the precursor used, culminating in differences in the crystal phases and the associated transitions, while the general perovskite crystal structure and composition is the same. The presence of the remaining excess CH_3NH_3Cl may suppress the phase transition in some fashion. The exact origin of these differences and the role of the Cl in the crystal structure of this perovskite are still under investigation.

The DSC thermogram displays peaks at 68.8 and 106.1 °C for the $PbCl_2$ case. The lack of these features in subsequent second cycles indicates that they may arise from the removal of excess solvent or absorbed H_2O from the perovskite powder. The different inorganic presursors used most likely have different affinity with the solvent and with water, hence resulting in different extents of residue traces within the material. This would explain the presence of such features in the $PbCl_2$ sample and not in the PbI_2 based material. Furthermore, the organic CH_3NH_3I precursor is highly hydrophilic, and hence, the $PbCl_2$ based case, which has a much higher organic content, might be more susceptible to water adsorption than the pure iodide mixture.

The transition at 106 °C has been attributed to the melting of the amorphous phase $(CH_3NH_3)_5PbCl_4I_3$ resulting from excess CH_3NH_3Cl.[24] Its loss at higher temperatures results in the disappearance of this feature in the second heating cycle. This process can be related to the different perovskite film morphologies observed when CH_3NH_3Cl is present.[13] Furthermore, some component of this phase could also contribute to the peak observed at 68.8 °C.

In this work, the thermal behavior of the perovskite was explored using TGA and DSC. The thermal properties of the individual components were used to gain knowledge of sublimation and/or decomposition mechanisms. Furthermore, the sublimation of the organic component was studied in depth as this process plays a critical role in the formation of the perovskite film during the heat treatment of the deposited perovskite solution. These results were used to correctly interpret the TGA curves of perovskite material formed from different mixtures. The sublimation of the excess organic product formed from mixed halide perovskite mixtures was observed as a separate process by TGA. The organic component of the perovskite decomposes by the subsequent loss of HI and CH_3NH_2 where the latter species is more tightly incorporated into the perovskite matrix. It is likely that this behavior may affect the long-term stability of these materials when used in solar cell applications. The tetragonal to cubic phase transition was observed only for the PbI_2 precursor based perovskite. These subtle differences in the formation process of the perovskite likely influence the photovoltaic performance of the material. The indicated flexibility to form the desired triiodide perovskite endorses us to fine tune the crystallization process. Furthermore, it provides insight into the thermal behavior and stability of the material, a useful parameter that needs to be considered for its application in solar cells.

dx.doi.org/10.1021/cm502468k | *Chem. Mater.* 2014, 26, 6160−6164

EXPERIMENTAL SECTION

Materials. All chemicals were purchased from Sigma-Aldrich and used as received. The organic components CH_3NH_3I and CH_3NH_3Cl were synthesized in our laboratory as reported.[1]

Sample Preparation. The precursor solution was prepared by dissolving the correct molar ratio of the organic (CH_3NH_3X) and the inorganic (PbX_2) components (where X is either Cl or I) in an appropriate solvent (DMF or DMSO) to give a 35 wt % solution.

To prepare the perovskite powder, the precursor solution was drop cast onto glass substrates and annealed at 100 °C until the as-deposited yellow film changed color to dark brown. This took approximately 10 min for the PbI_2 based perovskite (1:1 molar ratio of PbI_2 and CH_3NH_3I in DMF) and 45 min for the $PbCl_2$ based perovskite (1:3 molar ratio of $PbCl_2$ and CH_3NH_3I in DMF). The perovskite powder was scratched off the substrate and used directly for the thermal analysis. The powder was prepared under dry conditions.

Thermal Analysis. TGA was performed using TGA 4000 (PerkinElmer), heating at steady constant rates as specified (typically between 2.5 and 10 °C min^{-1}) under a constant 20 mL min^{-1} N_2 gas flow. The investigated temperature intervals were between a minimum of 30 °C to a maximum of 800 °C. Ceramic crucibles and approximately 5−15 mg of sample material were employed for each measurement.

DSC measurements were conducted using a DSC8000 (PerkinElmer) calorimeter at a rate of 10 °C min^{-1} from 30 to 200 °C under N_2. Approximately 2−5 mg of sample powder was used in each experiment using aluminum pans and lids. The data were recorded and analyzed using Pyris, Instrument Managing Software (PerkinElmer).

ASSOCIATED CONTENT

Supporting Information

Equation derivations, TGA curves of CH_3NH_3Cl at different heating rates, temperature profiles for isothermal measurements, calculated vapor pressure, TGA curves of perovskite solutions, and calculated wt % contributions of components to total perovskite mass. This material is available free of charge via the Internet at http://pubs.acs.org.

AUTHOR INFORMATION

Corresponding Author

*E-mail: michael.graetzel@epfl.ch.

Notes

The authors declare no competing financial interest.

ACKNOWLEDGMENTS

We thank K. Schenk for the XRD measurements and acknowledge financial support from Aisin Cosmos R&D Co., Ltd., Japan and from the European Community's Seventh Framework Programme (FP7/2007-2013) under "ORION" grant no. NMP-229036. This work was supported by the Global Research Laboratory (GRL) Program funded by the National Research Foundation in Korea. P.G. thanks the European Union Seventh Framework Programme (FP7/2007-2013) under grant agreement 'ENERGY-261920, ESCORT' and 308997 of the NANOMATCELL project.

REFERENCES

(1) NREL Record Cell Efficiencies. www.nrel.gov (accessed May 2014).
(2) Malinkiewicz, O.; Yella, A.; Lee, Y. H.; Espallargas, G. M.; Grätzel, M.; Nazeeruddin, M. K.; Bolink, H. J. *Nat. Photonics* **2014**, *8*, 128.
(3) Liu, M.; Johnston, M. B.; Snaith, H. *Nature* **2013**, *501*, 395.
(4) Ball, J. M.; Lee, M. M.; Hey, A.; Snaith, H. *Energy Environ. Sci.* **2013**, *6*, 1739.
(5) Eperon, G. E.; Stranks, S. D.; Menelaou, C.; Johnston, M. B.; Herz, L. M.; Snaith, H. *Energy Environ. Sci.* **2014**, *7*, 982.
(6) Edri, E.; Kirmayer, S.; Cahen, D.; Hodes, G. *J. Phys. Chem. Lett.* **2013**, *4*, 897.
(7) Shkrob, I. A.; Marin, T. W. *J. Phys. Chem. Lett.* **2014**, *5*, 1066.
(8) Noh, J. H.; Im, S. H.; Heo, J. H.; Mandal, T. N.; Seok, S. I. *Nano Lett.* **2013**, *13*, 1764.
(9) Jeng, J.-Y.; Chiang, Y.-F.; Lee, M.-H.; Peng, S.-R.; Guo, T.-F.; Chen, P.; Wen, T.-C. *Adv. Mater.* **2013**, *25*, 3727.
(10) Kim, H.-S.; Lee, J.-W.; Yantara, N.; Boix, P. P.; Kulkarni, S. A.; Mhaisalkar, S.; Grätzel, M.; Park, N.-G. *Nano Lett.* **2013**, *13*, 2412.
(11) Lee, M. M.; Teuscher, J.; Miyasaka, T.; Murakami, T. N.; Snaith, H. *Science* **2012**, *338*, 643.
(12) Burschka, J.; Pellet, N.; Moon, S.-J.; Humphry-Baker, R.; Gao, P.; Nazeeruddin, M. K.; Grätzel, M. *Nature* **2013**, *499*, 316.
(13) Zhao, Y.; Zhu, K. *J. Phys. Chem. C* **2014**, *118*, 9412.
(14) Wang, Q.; Dong, Q.; Xiao, Z.; Yuan, Y.; Huang, J. *Energy Environ. Sci.* **2014**, *7*, 2359−2365.
(15) Dualeh, A.; Tétreault, N.; Moehl, T.; Gao, P.; Nazeeruddin, M. K.; Grätzel, M. *Adv. Funct. Mater.* **2014**, *24*, 3250−3258.
(16) Eperon, G. E.; Burlakov, V. M.; Docampo, P.; Goriely, A.; Snaith, H. *Adv. Funct. Mater.* **2014**, *24*, 151.
(17) Wu, Y.; Yang, X.; Chen, H.; Zhang, K.; Qin, C.; Liu, J.; Peng, W.; Islam, A.; Bi, E.; Ye, F.; Yin, M.; Zhang, P.; Han, L. *Appl. Phys. Express* **2014**, *7*, 052301.
(18) Fahlman, B. D.; Barron, A. R. *Adv. Funct. Mater.* **2000**, *10*, 223.
(19) Langmuir, I. *Phys. Rev.* **1913**, *2*, 329.
(20) Vieyra-Eusebio, M. T.; Rojas, A. *J. Chem. Engineer. Data* **2011**, *56*, 5008.
(21) Yamada, K.; Nakada, K.; Takeuchi, Y.; Nawa, K.; Yamane, Y. *Bull. Chem. Soc. Jpn.* **2011**, *84*, 926.
(22) Colella, S.; Mosconi, E.; Fedeli, P.; Listorti, A.; Gazza, F.; Orlandi, F.; Ferro, P.; Besagni, T.; Rizzo, A.; Calestani, G.; Gigli, G.; De Angelis, F.; Mosca, R. *Chem. Mater.* **2013**, *25*, 4613.
(23) Baikie, T.; Fang, Y.; Kadro, J. M.; Schreyer, M.; Wei, F.; Mhaisalkar, S. G.; Grätzel, M.; White, T. J. *J. Mater. Chem. A* **2013**, *1*, 5628.
(24) Erk, P. Chemistry and Challenges of Soft Matter Based Solar Cells, HOPV14, Lausanne, Switzerland, 2014.